The Journal of Chemical Physics

Elucidation of pH Impacts on Monosubstituted Benzene Derivatives Using Normal Raman and Surface-Enhanced Raman Scattering

Wenjing Xi[1] and Amanda J. Haes[1, a)]
Chemistry Department, University of Iowa.

(Dated: 21 October 2020)

Raman spectral vibrational frequencies are used to probe the local chemical environment surrounding molecules in solution and adsorbed to gold nanostars. Herein, the impacts of functional group protonation on monosubstituted benzene derivatives with amine, carboxylic acid, or hydroxide are evaluated. Changes in binding affinity and orientation are apparent by evaluating systematic variations in vibrational frequencies. Notably, the electron donating abilities of these functional groups influence the vibrational frequency of the ring breathing mode thus leading to improved spectral interpretation. Furthermore, gold nanostars are used to investigate the impact of molecular protonation on the adsorption of benzoic acid/benzoate to gold. Changes in molecular protonation are measured using zeta potential and the surface-sensitive technique, surface-enhanced Raman scattering (SERS). These methods reveal that pH variations induce carboxylate protonation and electron redistribution that weaken molecular affinity thereby causing the molecule to adopt a perpendicular to parallel orientation with respect to the nanostar surface. Functional group identity influences the ring breathing mode frequency as a function of changes in electron donation from the functional group to the ring in solution as well as molecular affinity to and orientation on gold. This exploitation of vibrational frequencies facilitates the elucidation of molecule behavior in complex systems.

I. INTRODUCTION

Raman scattering is a complementary spectroscopic method to infrared (IR) absorption where incident photons excite vibrations resulting from changes in polarizability where the resulting spectra can be used for chemical species identification.[1] Vibrational frequencies can be modeled as a function of force constants and reduced mass of involved atoms;[2] however, experimental conditions such as solvent,[3] pH,[4] hydrogen bonding,[5] and bond order[6] can perturb the observed vibrational frequencies, intensities, and widths. Additionally, bond order, and as a result, vibrational frequencies, can be impacted by electronic resonance and inductive effects.[6] For instance, carbonyl absorbs IR energy at a lower frequency in 2-cyclohexenone than 2-pentanone because of variations in electron delocalization and a decrease in the double-bond character of the functional group.[7] Intermolecular interactions such as hydrogen bonding also influence the vibrational frequencies of chromophores in IR and Raman spectra. An example of this was highlighted in an experimental and theoretical investigation of 4-chlorobenzothiamide,[5] where the N-H stretching frequency red-shifted 5 cm^{-1} from intermolecular hydrogen bonding.

Similar effects are also observed in surface-enhanced Raman scattering (SERS) where normal Raman signals are enhanced via chemical and electromagnetic enhancement mechanisms[8] as well as surface selection rules.[9] For instance, changes in molecular polarizability perpendicular to an interface experience the greatest enhancement effects while parallel components are generally not enhanced.[10] Additionally, forbidden modes in normal Raman can be observed using SERS if the symmetry of the vibrational mode is perturbed upon interaction with a surface.[11, 12] Finally, molecule-surface interactions also influence vibrational frequencies. For example, the C-S stretching mode in L-cysteine is located at 672 cm^{-1} and 692 cm^{-1} in SERS and normal Raman spectra, respectively.[13] This 20 cm^{-1} red-shifted frequency upon adsorption to gold arises from electron donation from sulfur to gold.[13] This same trend is observed in SERS, and spectra calculated via DFT where charge transfer between triphenyl phosphine and silver causes this stretching frequency to red-shift in SERS vs. normal Raman scattering.[14]

Vibrational frequencies are sensitive to solution conditions and intermolecular interactions. Previously, vibrational frequencies were used to study hydrogen bonding between pyrimidine and various polar solvents,[15] adsorption geometries of molecules to surfaces,[16] and molecular orientation with respect to surfaces.[17] Mercury, for instance, was detected using SERS upon coordination to CN in a dimethyldithiocarbamic acid sodium salt.[18] As the Hg^{2+} concentration increased from 0-1 mM, the CN stretch shifted from 1374 to 1389 cm^{-1} as the ion interacted with sulfur.[18] Changes in vibrational frequency were more reproducible, sensitive, and selective vs. changes in intensity.[18] As such, this vibrational frequency–based detection was used in conjunction with purine and phenol as reporter molecules to quantitatively determine antigen concentration,[19] variations that were attributed to mechanical perturbations upon complex formation.[19]

In this work, we demonstrate that vibrational frequency variations in the ring breathing mode of monosubstituted benzene derivatives including anilinium/aniline, benzoic acid/benzoate, and phenol/phenoxide are sensitive to both local pH in solution as well as on plasmonic gold nanostars using normal Raman and SERS, respectively. This vibrational frequency is sensitive to the electron donating ability of the ring functional groups when the molecules are in solution while changes in molecular orientation are more apparent upon adsorption to gold. Vibrational frequencies associated with the ring breathing mode blue-shift as pH decreases because of changes in resonance and/or inductive effects as the

a)Electronic mail: amanda-haes@uiowa.edu.

functional group undergoes de/protonation. Next, the interaction of benzoic acid/benzoate to gold nanostars is evaluated as a function of carboxylate protonation using zeta potential and SERS spectral analysis. The vibrational frequencies of the ring breathing and the orientation-sensitive C-C stretching modes are studied as a function of pH and suggest that pH induces phenyl ring re-orientation. Finally, the binding affinity and molecular orientation of anilinium/aniline, phenol/phenoxide, and benzene on gold are explored using the vibrational frequency of the ring breathing mode. The pH-sensitive ring breathing mode frequency qualitatively suggests that the electron donating ability of the functional group significantly influences adsorption and molecular orientation on gold nanostars thereby leading to small yet reproducible and predictable changes in the measured vibrational spectra.

II. METHODS AND MATERIALS

A. Chemical Reagents

Gold (III) chloride trihydrate ($HAuCl_4 \cdot 3H_2O$), 4-(2-hydroxyethyl)-1-piperazineethanesulfonic acid (HEPES), benzene, benzoic acid, aniline, and phenol were purchased from Sigma Aldrich. Sodium hydroxide (NaOH), nitric acid (HNO_3), and ethanol were purchased from Fisher Scientific. Ultrapure water (18.2 $M\Omega \cdot cm^{-1}$) was obtained from a Barnstead Nanopure System (Dubuque, IA) and used throughout this study. All glassware was cleaned in a 3:1 HCl/HNO_3 solution and rinsed with water before drying in the oven.

B. Gold Nanostar Synthesis, Activation, and Characterization

Gold nanostars were synthesized according to previously published protocols.[20] Briefly, the pH of a 40 mM HEPES buffer was adjusted to 7.47 ($\pm$0.01) using NaOH yielding a final conductivity of 1150 μS/cm. Next, 200 μL of a 20 mM $AuCl_4$ aqueous solution was added to 20 mL of the HEPES buffer. After 10 seconds of agitation by hand to ensure homogeneous mixing, the solution remained undisrupted for 1 hour at 21 °C. The resulting gold nanostars were centrifuged (30 minutes, 2400xg) and supernatant removed, then sequentially dispersed in 20 and 10 mM HEPES buffer. The nanostars were stored in 10 mM HEPES at 4 °C until use. Prior to use, gold nanostars were washed and redispersed in water to disrupt the bilayer structure of HEPES on the gold nanostars.[21] Surface activation for SERS, whereby HEPES affinity to gold is weakened and/or desorbed, was completed by incubating 15 μL of gold nanostars (final concentration of 2 nM) in 135 μL of water that had been acidified to a pH of 3 using 1 M HNO_3 for 10 minutes. Nanostar concentration was estimated using extinction spectroscopy and a previously determined[22] extinction coefficient $\varepsilon_{\lambda_{max}}$ of 1.28 $nM^{-1} \cdot cm^{-1}$.

Gold nanostars were characterized using transmission electron microscopy (TEM, JEOL-1230 equipped with a Gatan CCD). To prepare samples, gold nanostars were diluted in ethanol by 50 % (v/v), then pipetted onto 400 mesh copper grids coated with Formvar and carbon (Ted Pella). Images were analyzed using Image Pro, and a minimum of 100 structures were evaluated for size estimations. The surface potential of pretreated (i.e., surface-activated) gold nanostars before and after incubation with benzoic acid was quantified using measured electrophoretic mobility at 25 °C with a Malvern Zetasizer (Worcestershire, UK). After surface activation, analytes were added to a solution containing nanostars so that final concentrations were 10 mM and 0.69 nM, respectively. A 1 M HNO_3 stock was added to vary pH from 0.9-3.2 for benzoic acid. Samples were prepared in triplicate and equilibrated for 3 minutes prior to data collection. Error bars represent the standard deviation of these data. Zeta potential was calculated using Henry's equation, measured mobilities, and calculated ionic strengths.[23]

C. Sample Preparation

Normal Raman spectra were collected using 25-60 mM benzoic acid/benzoate solutions prepared in water from pH 2.6 - 7.7, 220 mM aniline/anilinium in water from pH 1.3-8.1, or 0.9 M phenol/phenoxide in water from pH 8.7 - 11.4. SERS spectra were collected from 10 mM benzene (pH 1.0-3.5), benzoic acid (pH 0.9-4.0), aniline (pH 1.0 to 4.5), and phenol (pH 5.0-13.0). To increase molecular solubility, solutions were prepared so that each sample contained 2 % ethanol. This concentration of ethanol had a negligible effect on pK_a values. In addition, 1 M HNO_3 and/or NaOH solutions were used to adjust pH. Molecular solutions were prepared by adding 300 μL of an analyte stock solution to 150 μL of surface activated nanostars to final concentrations of 10 mM and 0.66 nM, respectively. Samples were vortexed for 10 seconds before all measurements. At the end of each measurement, pH was measured using pH paper (0.3 pH unit increments).

D. Normal Raman, SERS, and Extinction Spectroscopies

Normal Raman and SERS spectra (average = 3) were collected in triplicate using a semi-home built Raman microscope (ExamineR 785, DeltaNu) and fiber optically coupled laser (Integrated Photonic Solutions 785 nm) with an excitation wavelength (λ_{ex}) of 785 nm and tunable power (P) from 28-58 mW. Integration times (t_{int}) of 45 seconds was used for benzoic acid and benzoate (normal Raman), 30 seconds for all other normal Raman samples, and 25 seconds for SERS. Vibrational frequencies were determined from zero-point crossing values of first derivative normal Raman and SERS spectra. LSPR spectra were collected using an Ocean Optics vis-NIR spectrometer coupled with a tungsten-halogen light source. Spectral ranges varied from 390-1100 nm and were collected in triplicate using an integration time = 15 ms and average = 36. Gold nanostar concentration was determined using extinction magnitude at the maximum wavelength (λ_{max}), which was estimated from zero-point crossings of first derivative

spectra. Standard deviations of at least triplicate measurements are represented by error bars or as (±values).

E. DFT Calculations

Electrostatic potential energies were calculated for benzene derivatives in a water continuum to determine how electron distribution throughout the molecule was influenced by (de)protonation. Energy was first minimized using molecular mechanics theory calculations (Spartan '16, Version 2.0.7) and then calculations were performed in series ending with DFT B3LYP/6-31G*.

III. RESULTS AND DISCUSSION

A. Impact of Electron Delocalization on the Normal Raman Ring Breathing Mode of Monosubstituted Benzene Derivatives

Previously, the C-O stretching mode arising from monosubstituted phenol was shown to red-shift with increasing electron donation from the substituent group to the ring.[24] To evaluate the universality of these effects, normal Raman spectra are collected for anilinium/aniline, benzoic acid/benzoate, and phenol/phenoxide above and below their known solution pK_a values of 4.58 (-NH_2),[25] 4.19(-COOH),[26] and 9.95 (-OH).[27] We hypothesize that all vibrational mode frequencies from simple molecules such as mono-substituted benzene derivatives should red-shift with decreasing electron density in the functional moiety.

To study these pH dependent effects upon functional group (de)protonation, normal Raman spectra are collected, and vibrational frequencies are assigned then identified. Representative spectra and vibrational mode assignments for all chemical species are shown in Figure 1 and Table 1, respectively. Molecular concentrations that are used varied because of solubility and Raman cross section differences between protonated and deprotonated forms of a given molecule. All molecules show unique vibrational features associated with both the ring and functional groups. Furthermore, most of the vibrational features observed are related to the functional groups, and as a result, vary with protonation state. For example, a spectrum for benzoic acid (Figure 1A) reveals both C-C stretching (1602 cm^{-1}) and ring breathing (1003 cm^{-1}) modes while benzoate spectra (Figure 1B) contain these at 1600 and 1002 cm^{-1}, respectively, as well as carboxylate stretching (1390 cm^{-1}) and COO^- in-plane scissoring (841 cm^{-1}). Of note, the symmetric ring breathing mode,[28] which is typically centered at ~1000 cm^{-1}, varies in vibrational frequency for benzoic acid and benzoate and also for the other two molecular pairs. For example, this mode is located at 1006 cm^{-1} for anilinium (pH 1.3) but red-shifts to 1000 cm^{-1} for aniline (pH 8.0) as shown in Figures 1C and 1D, respectively, a response dependent on amine group protonation. A similar 7 cm^{-1} red-shift is noted upon deprotonation of phenol (Figures 1E and 1F).

FIG. 1. Normal Raman spectra and molecular structures of (A) benzoic acid (36 mM, pH 3), (B) benzoate (60 mM, pH 10), (C) anilinium (0.22 M, pH 1.3), (D) aniline (0.22 M, pH 8.1), (E) phenol (0.9 M, pH 8.7), (F) phenoxide (0.9 M, pH 11.4). Experimental Conditions: λ_{ex} = 785 nm, t_{int} = 45 s for benzoic acid/benzoate; t_{int} = 30 s for anilinium/aniline, phenol/phenoxide. P = 58 mW; average = 3. *Indicate non-analyte vibrational modes (see Table 1).

FIG. 2. pH-dependent vibrational frequency of the ring breathing mode using normal Raman spectroscopy. (A) Representative first derivative Raman spectra of aniline at pH (1) 8.1, (2) 5.2, (3) 4.9, (4) 4.5, and (5) 1.3. (B) pH-dependent ring breathing frequency relative to the most basic pH frequencies for (1) 900 mM phenol, (2) 200 mM aniline, and (3) 25 mM benzoic acid. Lines are fits using the derivative Henderson–Hasselbalch equation. (C) Comparison of the ring breathing mode frequency for benzene derivatives. pH was adjusted using 1 M HNO_3 or NaOH. Raman parameters: λ_{ex} = 785 nm, t_{int} = 30 s. and P = 58 mW. Error bars represent the standard deviation of three replicate measurements.

TABLE I. Vibration mode assignments (Raman and SERS).

Molecules	Raman, cm^{-1} (Lit.)	SERS, cm^{-1} (Lit.)	Raman, cm^{-1} (this work)	SERS, cm^{-1} (this work)	Assignment
HNO_3	1048	-	1046	-	NO_3 sym. str.[34]
HEPES	1280-1180	-	-	1255	C-N str.[35, 36]
	1310-1260	-	-	1288	CH_2 twist[24]
	1380	-	-	1347	SO_3 asym. str.[37, 38]
Benzoic Acid	1002	1002	1002	996	Ring breathing in phase[39, 40]
	-	1281	-	1285	C-O str.[39]
	-	1595	1602	1596	C-C str. of the benzene ring[41, 42]
Benzoate	-	836	841	835	COO^- in-plane scissoring[41]
	1002	1002	1003	1001	Ring breathing in-phase[39, 40]
	-	1370	1390	1372	COO^- sym. str.[39]
	-	1535	-	1539	COO^- asym. str. [41, 42]
	-	1595	1600	1596	C-C str. of the benzene ring[41, 42]
Aniline	541	-	-	533	NH_2 wagging[43]
	-	694	-	693	C-N bending/out of plane ring def.[44]
	817	-	815	798	Ring def.[44]
	998	-	1000	996	Ring breathing[43, 45]
	1029	-	1028	1027	NH_2 twist[45]/C-H bend[45]
	1176	-	-	1174	C-H bend[45]
	1265	-	1266	1228	C-N str. [44]
	1603	-	-	1594	C-C str. of the benzene ring[45]
Anilinium	541	-	-	529	NH_2 wagging[43]
	817	-	796	798	Ring def.[44]
	998	-	1006	994	Ring breathing[43, 45]
	1176	-	1179	1174	C-H bend[45]
	1265	-	-	1228	C-N str. [44]
Phenol	1001	993	1000	991	Ring breathing[46]
	1025	1018	1026	-	In-plane ring def. [46]
	1155	-	-	1114	C-H bend[47]
	1170	-	1172	1161	C-H bend[47]
	1242	-	1242	1252*	C-O str.[46]
	1263	1262	1268	-	C-O str.[46]
	1471	-	-	1446	Ring str.[47]
	1596	1579	1597	-	Ring str.[46, 47]
Phenoxide	992	984	993	993	Ring breathing[46]
	1108	-	-	1110	C-H bend[47]
	1155	-	1154	1150	C-H bend[47]
	1170	-	1168	-	C-H bend[47]
	-	1219	-	1222	C-O str.[48]
	1270	1273	1273	1253*	C-O str.[46]
	1471	-	-	1446	Ring str.[47, 48]
	1587	-	1585	-	Ring str.[46, 47]

[a] Overlaps with HEPES band.

In all cases, functional group protonation is hypothesized to cause the ring breathing mode to increase in energy upon decreasing electron donation of the functional group to the benzene ring. To investigate these effects, solution pH is systematically adjusted to decrease, and normal Raman spectra for these molecules are collected. The vibrational frequencies for the ring breathing mode are then analyzed using first derivative spectral analysis as shown in Figures 2A and reported as a function of pH (Figure 2B). The pH-dependent first derivative spectra for anilinium/aniline and representative zero-point crossing values for quantification of vibrational frequencies, are shown in Figure 2A as an example. This approach clearly distinguishes small variations in vibrational frequency[29] for the ring breathing mode that varies from 1006.0 to 999.2 cm^{-1} in the case of anilinium/aniline as pH increases from 1.3 to 8.1. Similar trends are observed for phenol (Figure 2B-1) and benzoic acid (Figure 2B-3). Because each functional group possesses a unique pK_a, the x-axis has been scaled so that "0" represents conditions in which pH = pK_a. By analyzing these data using the Henderson–Hasselbalch model, pK_a values are determined as 9.91 ($\pm$0.13), 4.71 ($\pm$0.07), and 3.68 ($\pm$0.14) for phenol, aniline, and benzoic acid, respectively, similar to previously reported values of 9.95,[27] 4.58,[27] and 4.19.[26] We attribute the slight variation in pK_a values for ani-

line and benzoic acid to differences in ion composition and or ionic strength.

For all molecules, the ring breathing mode for protonated benzene derivatives are higher in energy than the deprotonated molecular versions, an effect we attribute to both inductive and resonance effects. Previously, delocalization indices were developed to describe the probability of finding electron pairs in space as a function of inductive and resonance effects.[6] Resonance effects can influence vibrational frequencies through π electron perturbation whereas inductive effects arise from electrons in σ orbitals. Because both COOH and COO^- serve as electron withdrawing groups to the phenyl ring and are dominated by resonance effects, variations in the vibrational frequency for the ring breathing mode are small (~0.8 cm^{-1} change). In contrast, both NH_3^+/NH_2 and OH/O^- exhibit variations via inductive effects and more significant changes in electron delocalization than carboxylate/carboxylic acid (i.e., NH_3^+ is electron withdrawing while NH_2 is electron donating). As a result, protonation induces a 7.6 and 8.5 cm^{-1} shift in the ring breathing mode vibrational frequency, respectively. These results are similar to previous studies that revealed that C=C stretching vibrations associated with alkenes are also sensitive to functional group protonation.[24, 30]

Collectively, these data suggest that functional group electron donation systematically impacts the ring breathing mode vibrational frequency. As shown in Figure 2C, the vibrational frequency red-shifts with increasing electron donation to the phenyl ring (i.e., $NH_3^+ < COOH < COO^- < H < OH < NH_2 < O^-$).[31] These results can be understood in terms of delocalization indices.[6] As the electron withdrawing capabilities of the functional group decrease (i.e., from NH_3^+ to NH_2), electrons become more delocalized from the phenyl ring (i.e., decrease in delocalization index)[6] causing the associated force constant to decrease[32, 33] and vibrational frequency to red-shift from 1006 to 1000 cm^{-1}. While these effects are strongest for the ring breathing mode, other vibrational features including the in-plane ring deformation show similar behavior in that a 5 cm^{-1} red-shift is observed upon functional group deprotonation. This suggests that all intermolecular interactions have the potential to influence vibrational frequencies including those observed in SERS (*vide infra*).

B. Impact of Molecular Protonation on the Adsorption of Benzoic Acid to Gold Nanostars

Now that impacts of molecular protonation on normal Raman vibrational frequencies for monosubstituted benzene derivatives have been identified, resulting implications on molecular adsorption and SERS can be extracted. Previous studies suggest that functional group protonation generally weakens molecular binding affinity to a metal interface[16, 49] and influences surface orientation.[16] To investigate these effects on gold nanostar surfaces, the implication of functional group protonation on the adsorption and orientation of benzoic acid/benzoate is evaluated using SERS. We focus on this benzene derivative because the carboxylic acid group undergoes ionic and covalent coordination interactions with gold[50] and de/protonation of this group changes little in its electron withdrawing nature as discussed in the previous section. Thus, all SERS spectral changes arise from variations in molecule-surface interactions and orientation effects at the interface.

To study these effects, gold nanostars are used because of their ideal plasmonic properties for 785 nm excitation for SERS and straight-forward surface activation for the adsorption of non-thiolated benzene derivatives.[21] As shown in Figure 3A, LSPR spectra associated with gold nanostars before and after surface activation with HNO_3 initially contain two plasmonic features centered at 518 and 692 nm, which arise from hybridized resonances associated with the nanostar core and branches,[51] respectively. As shown in Figure 3A-2 and in the inset, the optical properties and morphology of gold nanostars are retained upon surface activation. Notably, only a slight 3 nm blue shift is observed in the low energy plasmon mode, a result consistent with slight morphological restructuring of the nanostars.[21] Upon acidification, the gold nanostar morphology and surface activation are retained for ~90 minutes, so the materials were used within this time frame for all subsequent experimental measurements. It should be noted that HEPES affinity to gold increases with longer incubation times thus requiring repeated activation through acidification prior to SERS assays.

Because adsorption causes the pK_a of carboxylic acids to decrease, the surface pK_a ($pK_{a,surf}$) for the carboxylic acid group in the molecule must be determined. To do so, stock solutions of benzoic acid/benzoate (pH 0.9 – 4.0) are added to gold nanostars to final concentrations of 10 mM and 0.69 nM, respectively. After equilibration, both zeta potential and SERS are measured as a function of pH as shown in Figures 3B and 3C, respectively. To aid in surface pK_a quantification, log values of zeta potential are calculated to linearize the response. As pH increases, log(-zeta potential) values increase linearly then saturate. The estimated $pK_{a,surf}$ value for the carboxylate group occurs at the intersection of these two regimes[29] and is 2.17 ($\pm$0.3). This value is reasonable when considering the previously published bond strength of C=O to gold (-9.2 kJ/mol (-2.2 kcal/mol))[52, 53] and the solution pK_a of the carboxylic acid group estimated from the Raman data in the previous section (3.68 ($\pm$0.14)). This is achieved by estimating the $pK_{a,surf}$ as follows:[54]

$$pK_{a,surf} = \frac{\Delta G^\circ}{2.303RT} + pK_{a,soln}$$

where ΔG° is the change in Gibbs free energy associated with adsorption of the functional group to the gold nanostar surface, R is the gas constant, and T is temperature (298 K). This calculation estimates a $pK_{a,surf}$ of 2.04 ($\pm$0.14), a value not statistically different from the experimentally determined value from zeta potential measurements.

SERS analysis suggests that benzoate displaces HEPES upon adsorption. These data are summarized as a function of time in Figure S1 and as a function of pH in Figures 3C and 3D. In all cases, SERS spectra are collected using 10 mM benzoic acid/benzoate that is incubated with 0.69 nM activated gold nanostars. SERS signals arise primarily from molecules

The Journal of Chemical Physics

FIG. 3. pH-dependent zeta potential and SERS analysis of benzoic acid/benzoate using 2 nM gold nanostars. (A) Representative LSPR spectra of gold nanostars (1) before and (2) after surface activation (1 mM HNO_3 for 10 minutes). Inset shows TEM images of gold nanostars. (B) Surface pK_a of benzoic acid on gold nanostars evaluated as a function of log(-zeta potential (mV)). (C) Representative SERS spectra of 10 mM benzoic acid at pH of (1) 3.0, (2) 2.8, (3) 2.5, (4) 2.2, and (5) 1.2 in 0.69 nM activated gold nanostars. (D) SERS signal of the (1) normalized C-O stretch (1285 cm^{-1}) and (2) relative C-C stretch (1596 cm^{-1}) (relative to ring breathing (1000 cm^{-1})). Error bars represent the standard deviation of three replicate measurements. Estimated surface pK_a values are 2.17 ($\pm$0.30), 2.30 ($\pm$0.02), and 1.81 ($\pm$0.17) using zeta potential, normalized SERS signal of C-O stretch, and C-C stretch, respectively. Errors in pK_a values are estimated from uncertainties in linear fittings for log (-zeta potential). Sigmoidal model is used in SERS and pK_a values are estimated form zero-crossing point in the second derivative spectra of SERS analysis. SERS parameters: λ_{ex} = 785 nm, t_{int} = 25 s. and P = 58 mW, and average = 3. Bands labeled with * represent vibrational modes from solution: NO_3 symmetric stretch from HNO_3 (1046 cm^{-1}) and C-C-O stretch from 2% ethanol (877 cm^{-1}).

adsorbed at positive curvature features on the nanostars (i.e., branch tips).[55] The time-dependent SERS signals (Figure S1) suggest benzoic acid/benzoate adsorption reaches equilibrium within 1 minute regardless of solution pH, a result that is reasonable given the relatively high molecular concentration vs. nanostars. As a result and because nanostar instability begins to influence spectral intensities after 10 minutes, only SERS spectra collected within five minutes are analyzed. Representative SERS spectra collected from pH 1.2-3 are shown in Figure 3C. All vibrational features arise from benzoic acid/benzoate except those centered at 1046 and 877 cm^{-1}, which are the NO_3 symmetric stretch from HNO_3[34] and the C-C-O stretch from 2 % ethanol, respectively.[56] Notably, no vibrational features associated with HEPES are observed (see prior studies for reference spectra[21]) thereby suggesting benzoate displaces the surface stabilizing agent upon adsorption.

The vibrational modes observed using SERS for benzoate/benzoic acid are pH dependent and exhibit enhancement factors vs. normal Raman spectra of ~10^4. These are most apparent from changes in the ring breathing, COO^- in plane scissoring, and C-O stretching (in COOH) modes. Several observations are noted. First, the most intense vibrational feature in all of these spectra arises from the ring breathing mode (1000 cm^{-1}).[39, 40] This band decreases by over 150 % with decreasing pH, a result consistent with more energetically favorable binding and larger surface density of adsorbed carboxylate vs. carboxylic acid groups to gold. Second, both the COO^- in-plane scissoring (834 cm^{-1})[41] and C-O stretch in COOH (1285 cm^{-1})[39] are also observed, but their relative intensities vary with pH. For instance, only the C-O stretch (1285 cm^{-1}) is observed at pH 1.2 while both modes are observed at all other pHs. As pH increases, the COO^- in-plane scissoring mode (834 cm^{-1}) increases in intensity suggesting that molecular deprotonation impacts both resulting adsorption energy as well as molecular orientation on gold. Third, the C-O stretching (1285 cm^{-1}) intensity increases by 20 % with increasing pH. Because this signal variation is smaller than that observed for the ring breathing mode, we hypothesize that both molecular density and orientation are changing with pH. To carefully evaluate these data, the normalized C-O stretching signal (i.e., integrated area) vs. pH is analyzed as shown in Figure 3D-1. As pH increases, the relative signal for the C-O stretch, which represents the molecular surface density of benzoic acid, decreases and exhibits a surface $pK_a = 2.3_0$ ($\pm 0.0_2$), a value in good agreement with the estimated surface pK_a (2.2 ($\pm$0.3)) from zeta potential. Slight variations in the observed surface pK_a values likely arise from influences from residual HEPES molecules (3.8 ($\pm$0.2));[21] however, similar trends are noted.

Furthermore, we hypothesize that the binding affinity of the functional group weakens from benzoate to benzoic acid, which also changes molecular orientation because of a decrease in molecular surface density as well as variations in adsorption driving forces. This is similar to what is observed for α-cyano-4-hydroxycinnamic acid on silver[16] where basic pH conditions promoted carboxylate binding and a parallel orientation of the C-N group with respect to the surface while C-N oriented in a perpendicular orientation in acidic conditions because of the weakened affinity of carboxylic acid vs. C-N.

To investigate these effects for benzoic acid/benzoate on gold nanostar surfaces, the orientation-sensitive C-C stretching mode (1596 cm^{-1}) is evaluated as a functional of pH. The C-C stretch should exhibit maximum enhancement when oriented perpendicular to the Au surface according to surface selection rules.[57] As shown in Figure 3D-2, this signal is reported relatively to the ring breathing mode so that the differences in surface molecular density can be removed from this analysis. The relative SERS signal increases with increasing pH and exhibits an inflection point at a pH of 1.8 ($\pm$0.2). This value is close to the estimated surface pK_a (2.17 ($\pm$0.30)) and indicates molecular tilt angle depends on pH. When pH is above the surface pK_a, carboxylate binds to gold resulting in the ring oriented perpendicularly to the surface while in so-

FIG. 4. Representative first-derivative SERS spectra of 10 mM (A) benzoic acid/benzoate, (B) anilinium/aniline, (C) phenol/phenoxide, and (D) benzene using 0.69 nM gold nanostars in aqueous solution as a function of pH. A 6 cm^{-1} range is shown for each sample. A: pH = (1) 2.5, (2) 2.2, (3) 1.8, and (4) 1.5. B: pH = (1) 3.6, (2) 3.1, (3) 2.5, and (4) 1.7. C: pH = (1) 7.0, (2) 9.5, (3) 11.8, and (4) 12.1. D: pH = (1) 1.6, (2) 2.0, (3) 2.5, and (4) 3.0. SERS parameters: λ_{ex} = 785 nm, t_{int} = 25 s. and P = 58 mW, and average = 3.

lution with pH values that are below the surface pK_a leads to benzene rings lying flat[21] on gold to maximize π orbital-gold overlap.

C. Using SERS and the Ring Breathing Frequency to Understand Changes in Binding Affinity and Orientation of Benzoic Acid/Benzoate, Anilinium/Aniline, Phenol/Phenoxide, and Benzene

As established in Figures 1-2, functional group protonation induces a blue-shift in the ring breathing mode for benzene derivatives in solution while a red-shift is observed in SERS. As shown in Figure 4, this is observed for benzene as well as benzoic acid/benzoate, anilinium/aniline, and phenol/phenoxide. Zero-point crossings of first derivative spectra are shown to carefully distinguish these small but reproducible spectral changes. For instance, the vibrational frequency of the ring breathing mode systematically red shifts from 1001.3 to 996.5 cm^{-1} as pH decreases from 2.5 (above the surface pK_a) to 1.5 for benzoic acid/benzoate (Figure 4A). This red-shift is consistent with molecular reorientation from a nearly perpendicular orientation with respect to the metal to parallel.[58] Similar red-shifts were observed previously for the C-N stretching frequency in which π orbital overlap with silver occurred when the bond was parallel to the surface.[16] To further investigate this behavior for benzene derivatives, SERS spectra are collected for anilinium/aniline, phenol/phenoxide, and benzene by varying the pH above and below the functional group pK_a. Solution pK_a values of 4.58(-NH_2)[25] and 9.95 (-OH)[27] for aniline and phenol, respectively, guided initial solution pH ranges to determine surface pK_a values. The relevant ranges are pH 1.3-4.3 and 5.0-12.5 for anilinium/aniline and phenol/phenoxide, respectively. The representative first derivative spectra near the ring breathing mode frequencies and the entire SERS spectra are shown in Figures 4B-C and Figure 5, respectively. Both aniline and phenol behave similarly to benzoic acid. The ring breathing mode red shifts 3.5 and 2.1 cm^{-1}, for aniline and phenol, respectively, as pH decreases. These small yet discernible red-shifts are attributed to variations in molecular orientation and are in contrast to the 8 cm^{-1} blue shifts in vibrational frequency observed upon functional group protonation for both molecules in solution. Vibrational frequency sensitivity to molecular orientation is confirmed by analyzing trends with respect to benzene. The pH sensitive ring breathing mode for this control molecule are shown in Figure 4D where the vibrational frequency varies randomly at 966 cm^{-1} without any trend as pH is varied from 1.6-3. This indicates that neither ionic strength nor nitric acid concentration (i.e., pH) affect the ring breathing frequency for benzene as well as for all other benzene derivatives used in this study. Complete spectra for both aniline/anilinium and phenoxide/phenol are shown in Figure 5. Vibrational band assignments are summarized in Table 1 and are mostly high symmetry modes that are sensitive to electromagnetic enhancement. Similar to the normal Raman results, both phenyl ring and functional group modes in the SERS spectra depend on functional group protonation. For instance, Figure 6 summarizes the relative trends for the ring breathing frequency for all of the benzene derivatives studied here (relative to the most acidic sample). Two trends are noted. First, phenol exhibits the smallest pH dependence in ring breathing mode frequency with only a 2 cm^{-1} red-shift with decreasing pH, a result that is attributed to the weak affinity between hydroxyl and gold. As a result and as depicted in Figure 7, phenol/phenoxide likely interacts with gold via the ring resulting in a parallel, pH-independent orientation. This is confirmed by the lack of the C-C stretch observed for the ring in the SERS spectra. As such, both molecules (phenol and phenoxide) exhibit binding affinities similar yet slightly weaker than for benzene (3.69 ($\pm$0.06) kcal/mol)[21] because the functional groups donate electrons to the phenyl ring thereby weakening its affinity to gold. Second, the ring breathing mode frequency changes significantly for both benzoic acid/benzoate and anilinium/aniline by ~2.4 and 2.6 pH units below their solution pK_a, respectively. This indicates that gold interactions influence the electron distribution of the carboxylic acid and amine groups. Of note, a larger decrease in pK_a should be observed for aniline as the primary amine binds to gold with a binding affinity of 6-8 kcal/mol,[52, 59] which is ~3 times larger than benzoate to gold. As summarized in Figure 7, the ring breathing mode frequency red-shifts in SERS as pH decreases because the molecules align in a parallel orientation with respect to gold upon functional group protonation, a result very similar to benzene. In contrast, both benzoate and aniline interact with gold through their func-

6.png

FIG. 5. SERS spectra of 10 mM (A) (1) aniline (pH 4.3) and (2) anilinium (pH 1.3) and (B) (1) phenoxide (pH 11.2) and (2) phenol (pH 5). SERS parameters: λ_{ex} = 785 nm, t_{int} = 25 s, P = 58 mW, average = 3. *887 cm^{-1} and *1046 cm^{-1} represent C-C-O stretch from 2% ethanol and NO_3 symmetric stretch from HNO_3, respectively. *1348 cm^{-1} and *1288 cm^{-1} are from HEPES and summarized in Table 1.

FIG. 6. Relative ring breathing mode frequency (vs. the most acidic measurement) for (1) benzoic acid/benzoate, (2) anilinium/aniline, (3) phenol/phenoxide, and (4) benzene as a function of pH (pH 5-12 for phenol and 0-4.5 for others). A sigmoidal fit is included for (1), (2), and (3). Linear fitting is applied to data set (4). SERS parameters: λ_{ex} = 785 nm, t_{int} = 25 s, P = 58 mW, average = 3. The error bars represent the standard deviation of three replicate measurements.

tional groups rather than through their rings. This induces significant changes in vibrational frequency because of the resulting orientation changes. Because NH_3^+ and COO^- are electron withdrawing groups with poor affinities to gold, these monosubstituted benzene derivatives exhibit stronger affinity to gold (than benzene) through π-Au orbital overlap.

IV. CONCLUSIONS

In summary, functional group (COO^-, NH_2, O^-) protonation for monosubstituted benzene derivatives leads to a red-shift in the ring breathing mode frequencies observed in SERS as pH decreases. This effect is attributed to a decrease in binding affinity between the functional group and gold upon protonation, which subsequently causes the molecules to adopt more parallel geometries on gold relative to their deprotonated molecular forms. These effects were identified after rigorously determining that this same vibrational frequency blue-shifts upon functional group protonation (i.e., near the pK_a) in normal Raman measurements, variations induced from both large inductive (aniline and phenol) and small resonance (carboxylic acid) effects from functional group protonation. Namely, both aniline and phenol showed ~8 cm^{-1} blue-shifts while benzoic acid only showed a ~1 cm^{-1} blue-shift upon decreasing pH below the pK_a. Acidification of the surface pK_a of benzoic acid by ~2 pH units was quantified by measuring changes in its ring breathing mode, a result confirmed using a standard method (i.e., zeta potential). Furthermore, the ring breathing mode frequency for benzoic acid red-shifted 5 cm^{-1} upon decreasing pH near the estimated surface pK_a, indicating reorientation from a perpendicular to flat orientation, a result confirmed using the orientation-sensitive C-C stretching vibrational mode. Similar trends were observed for for anilnium/aniline but not phenol/phenoxide and benzene. These studies suggest that changing the simple parameter of pH can have profound impacts on vibrational spectral features, results that can be understood in terms of both surface selection rules and electron density.

V. SUPPLEMENTARY MATERIAL

See supplemental material for time dependent SERS spectra and analysis for benzoate.

ACKNOWLEDGMENTS

This work is supported by the National Science Foundation (DMR-1707859). This research was facilitated by the IR/D (Individual Research and Development) program associated with AJH's appointment at the National Science Foundation.

FIG. 7. Proposed structures and orientation of benzoic acid, aniline, and phenol on gold nanostars.

VI. DATA AVAILABILITY

The data that support the findings of this study are available from the corresponding author upon reasonable request.

VII. REFERENCES

[1] J. C. Lindon, G. E. Tranter, and D. Koppenaal, Encyclopedia of Spectroscopy and Spectrometry (Academic Press, 2016),
[2] in Interpreting Infrared, Raman, and Nuclear Magnetic Resonance Spectra, edited by R. A. Nyquist (Academic Press, San Diego, 2001).
[3] S. Dutta et al., ACS Appl. Mat. Interf. **5**, 8724 (2013).
[4] J. M. Delabar, J. Raman Spect. **7**, 261 (1978).
[5] A. A. Howard, G. S. Tschumper, and N. I. Hammer, J. Phys. Chem. A **114**, 6803 (2010).
[6] C. Outeiral et al., Chem. Sci. **9**, 5517 (2018).
[7] D. Lin-Vien et al., The Handbook of Infrared and Raman Characteristic Frequencies of Organic Molecules (Elsevier, 1991).
[8] G. Demirel et al., J. Mat. Chem. C **6**, 5314 (2018).
[9] P. Cao, R. Gu, and Z. Tian, J. Phys. Chem. B **107**, 769 (2003).
[10] H. K. Turley et al., J. Phys. Chem. Lett. **8**, 1819 (2017).
[11] M. Moskovits, D. DiLella, and K. Maynard, Langmuir **4**, 67 (1988).
[12] J. R. Lombardi, Faraday Discuss. **205**, 105 (2017).
[13] C. Jing, and Y. Fang, Chem. Phys. **332**, 27 (2007).
[14] G. Hu et al., J. Phys. Chem. C **111**, 8632 (2007).
[15] A. M. Wright et al., J. Phys. Chem. A **117**, 5435 (2013).
[16] D. Jung et al., Appl. Surf. Sci. 63 (2017).
[17] X. Wang et al., Anal. Chem. **88**, 915 (2015).
[18] L. Chen et al., Analyst **141**, 4782 (2016).
[19] K. W. Kho et al., ACS Nano **6**, 4892 (2012).
[20] J. Xie, J. Y. Lee, and D. I. Wang, Chem. Mater. **19**, 2823 (2007).
[21] W. Xi, and A. J. Haes, J. Am. Chem. Soc. **141**, 4034 (2019).
[22] H. de Puig et al., J. Phys. Chem. C **119**, 17408 (2015).
[23] H. Ohshima, J. Colloid Interface Sci. **168**, 269 (1994).
[24] G. Socrates, Infrared and Raman Characteristic Group Frequencies: Tables and Charts (Wiley, 2001).
[25] K. C. Gross et al., J. Org. Chem. **66**, 6919 (2001).
[26] E. V. Soriano et al., Biochem. **47**, 1346 (2008).
[27] A. Kütt et al., J. Org. Chem. **73**, 2607 (2008).
[28] I. Hyams, R. Bailey, and E. R. Lippincott, Spectrochim. Acta A **23**, 273 (1967).
[29] W. Xi et al., J. Phys. Chem. C **122**, 23068 (2018).
[30] B. Giese, and D. McNaughton, J. Phys. Chem. B **106**, 101 (2002).
[31] R. O. C. Norman, and R. Taylor, Electrophilic Substitution in Benzenoid Compounds (Elsevier, 1965), Vol. 3.
[32] G. E. Maciel, and J. J. Natterstad, J. Chem. Phys. **42**, 2752 (1965).
[33] R. Stewart, and K. Yates, J. Am. Chem. Soc. **82**, 4059 (1960).
[34] Y.-C. Liu et al., Thin Solid Films **374**, 85 (2000).
[35] D. L. Pavia, G. M. Lampman, and G. S. Kriz, (Harcourt Brace College Publishers).
[36] J. S. Kumar et al., Spectrochim. Acta A **152**, 509 (2016).
[37] S. Y. Tang, and C. W. Brown, J. Raman Spect. **3**, 387 (1975).
[38] D. S. Warren, and A. J. McQuillan, J. Phys. Chem. B **112**, 10535 (2008).
[39] X. Gao, J. P. Davies, and M. J. Weaver, J. Phys. Chem. **94**, 6858 (1990).
[40] K. Zheng et al., J. Raman Spect. **41**, 632 (2010).
[41] J. Gao et al., Spectrochim. Acta A **104**, 41 (2013).
[42] M. Pagannone, B. Fornari, and G. Mattei, Spectrochim. Acta A **43**, 621 (1987).
[43] P. M. Wojciechowski et al., J. Chem. Phys. **118**, 10900 (2003).
[44] A. Blacha-Grzechnik et al., Vib. Spectrosc. **71**, 30 (2014).
[45] J. C. Evans, Spectrochim. Acta **16**, 428 (1960).
[46] M. Fleischmann et al., Electrochim. Acta **28**, 1545 (1983).
[47] J. Evans, Spectrochim. Acta **16**, 1382 (1960).
[48] N. Ornelas-Soto et al., in 3rd International Conference on Applications of Optics and Photonics (International Society for Optics and Photonics, 2017).
[49] K. R. Karnati, and Y. Wang, PCCP **20**, 9389 (2018).
[50] F. Chen et al., J. Am. Chem. Soc. **128**, 15874 (2006).
[51] F. Hao et al., Nano Lett. **7**, 729 (2007).
[52] F. Tarazona-Vasquez, and P. B. Balbuena, J. Phys. Chem. B **108**, 15992 (2004).
[53] J.-W. Park, and J. S. Shumaker-Parry, J. Am. Chem. Soc. **136**, 1907 (2014).
[54] S. M. Ansar et al., J. Phys. Chem. C **117**, 8793 (2013).

[55] G. Lu, T. Z. Forbes, and A. J. Haes, Analytst **141**, 5137 (2016).
[56] S. Burikov et al., Mol. Phys. **108**, 2427 (2010).
[57] W. Xi, B. K. Shrestha, and A. J. Haes, Anal. Chem. **90**, 128 (2018).
[58] P. Gao, and M. J. Weaver, J. Phys. Chem. **89**, 5040 (1985).
[59] R. Di Felice, and A. Selloni, J. Chem. Phys. **120**, 4906 (2004).

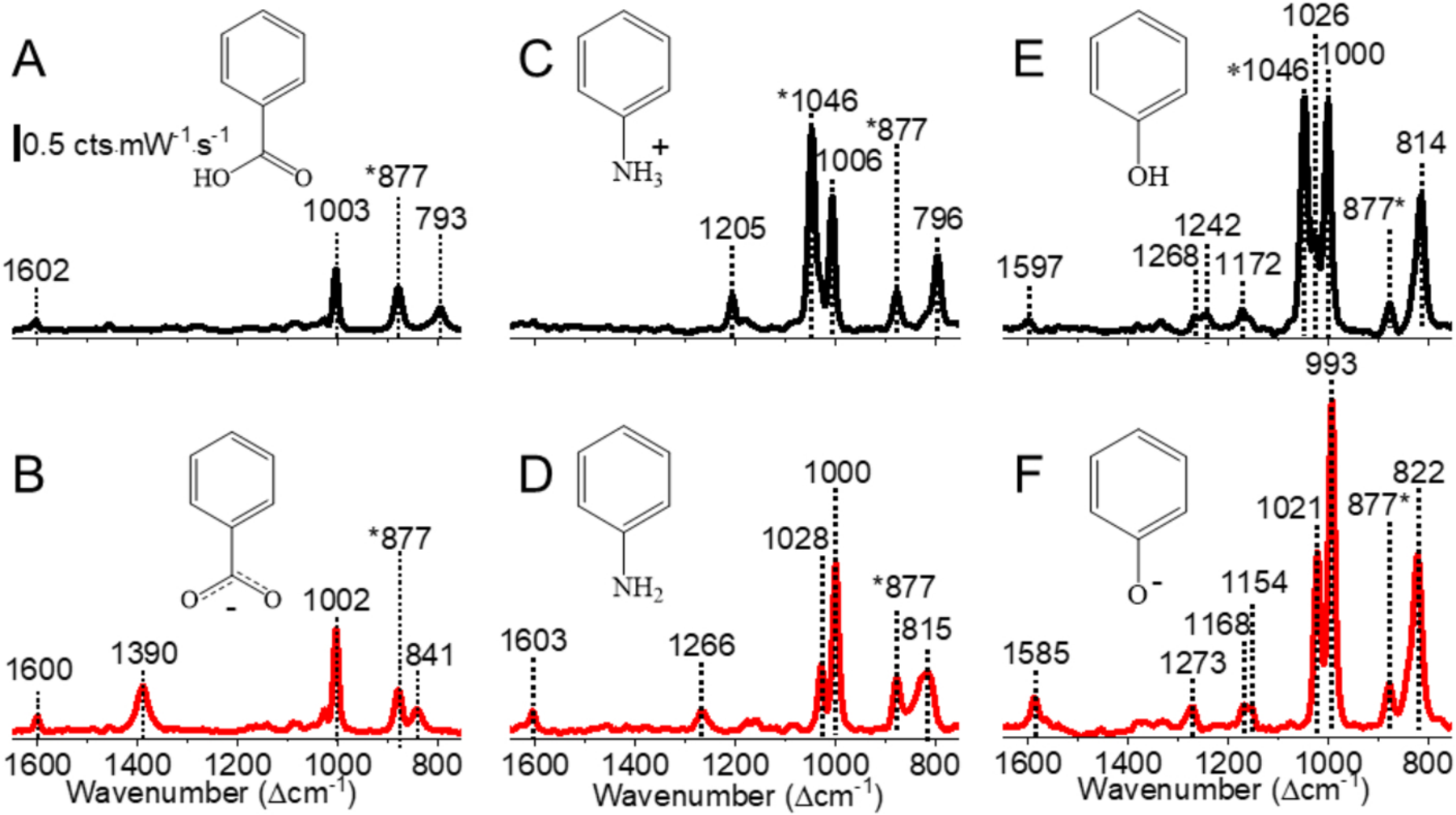
A
0.5 cts·mW-1·s-1
HO
O
1602
1003
*877
793
B
O
-
O
1600
1390
1002
*877
841
C
NH3
+
1205
*1046
1006
*877
796
D
NH2
1603
1266
1028
1000
*877
815
E
OH
1597
1268
1242
1172
*1046
1026
1000
877*
814
F
O-
1585
1273
1168
1154
1021
993
877*
822
1600 1400 1200 1000 800
Wavenumber (Δcm-1)

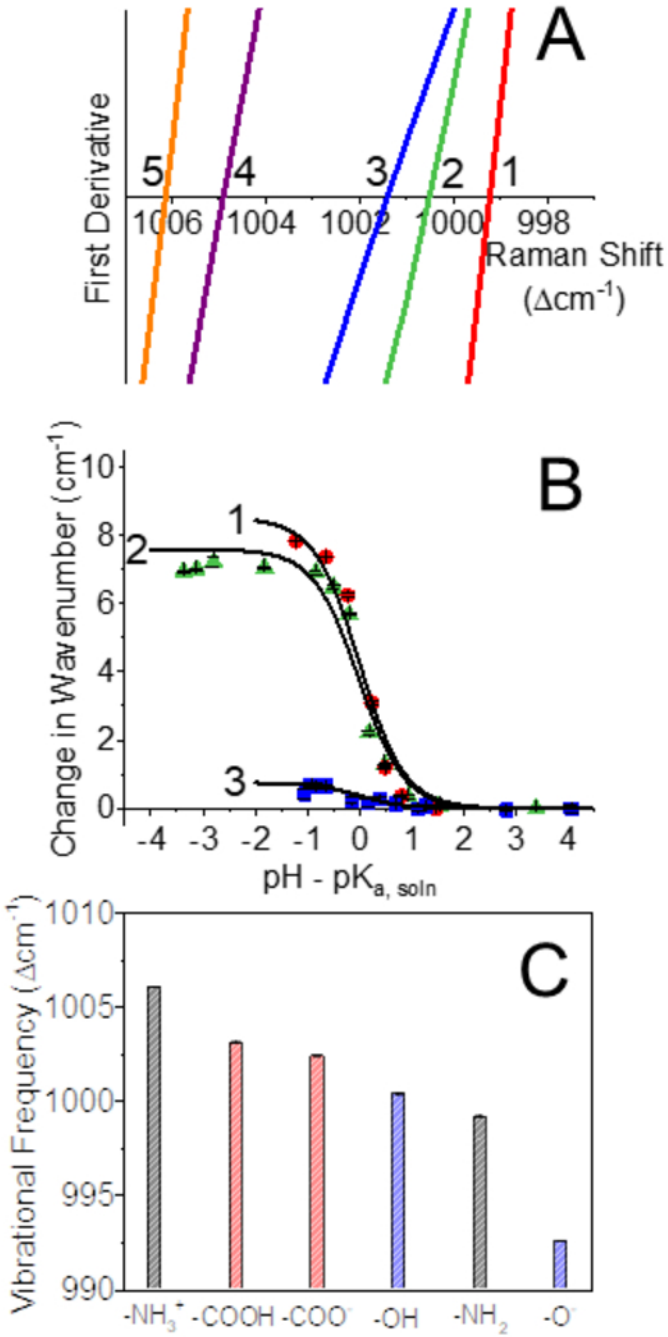
A
First Derivative
5
4
3
2
1
1006
1004
1002
1000
998
Raman Shift
(Δcm-1)
B
Change in Wavenumber (cm-1)
10
8
6
4
2
0
1
2
3
-4
-3
-2
-1
0
1
2
3
4
pH - pKa, soln
C
Vibrational Frequency (Δcm-1)
1010
1005
1000
995
990
-NH3+
-COOH
-COO-
-OH
-NH2
-O-

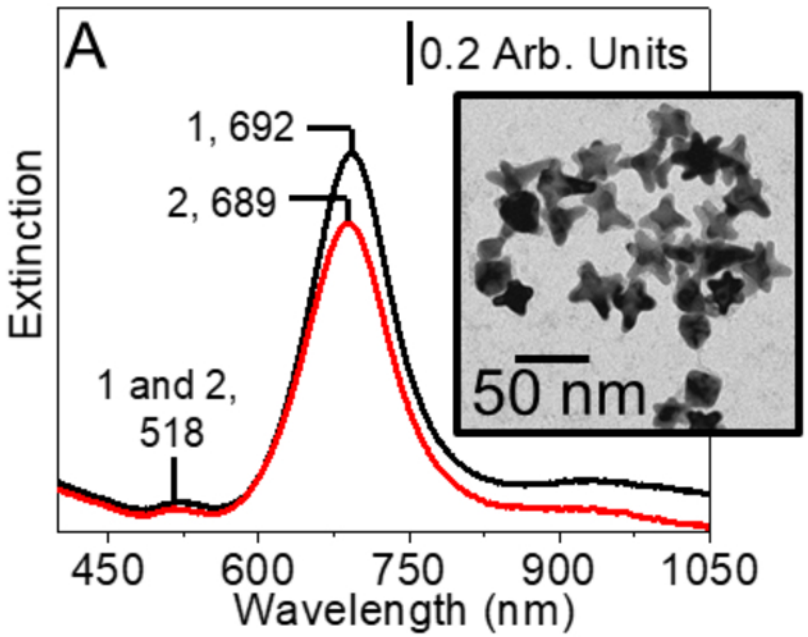
A
0.2 Arb. Units
1, 692
2, 689
1 and 2,
518
50 nm
Extinction
450
600
750
900
1050
Wavelength (nm)

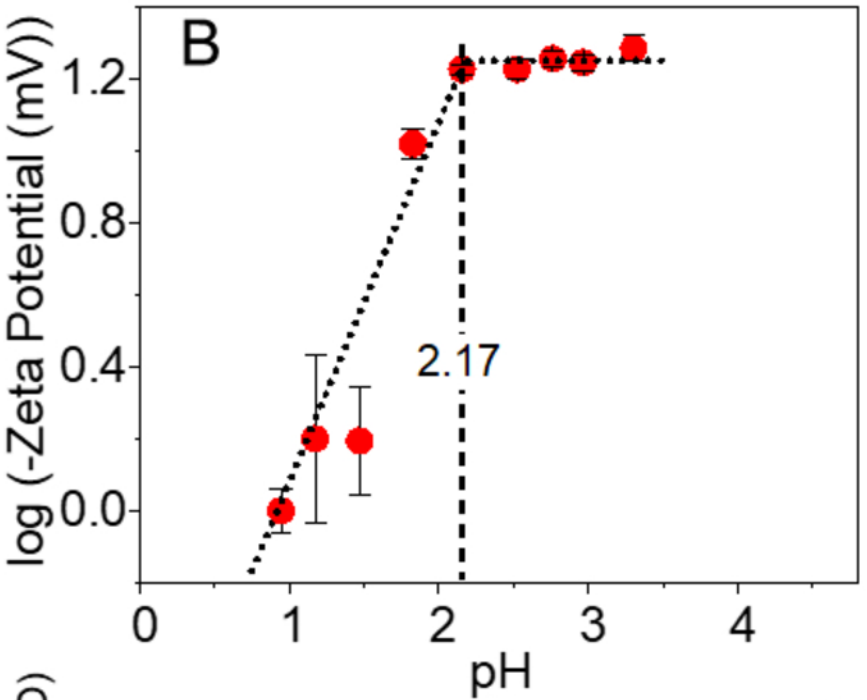
B
log (-Zeta Potential (mV))
1.2
0.8
0.4
0.0
2.17
0
1
2
3
4
pH

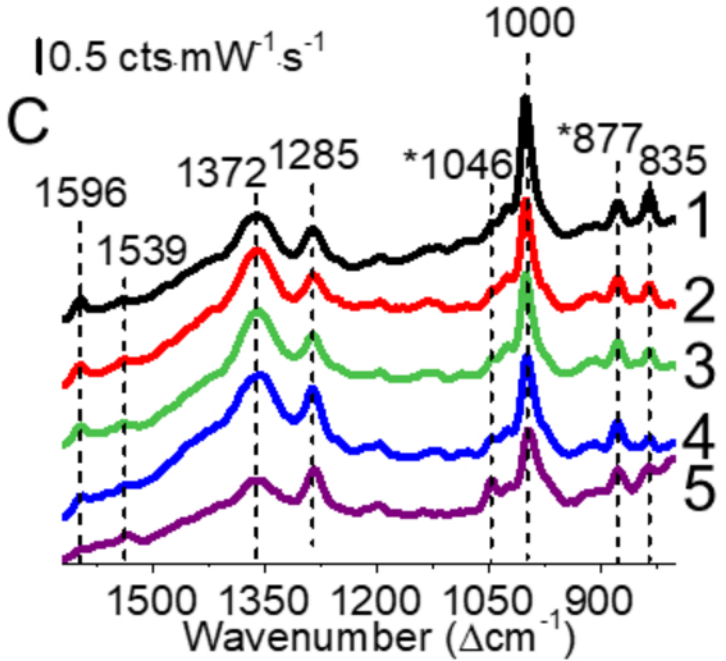
0.5 cts·mW-1·s-1
C
1000
1596
1539
1372
1285
*1046
*877
835
1
2
3
4
5
1500
1350
1200
1050
900
Wavenumber (Δcm-1)

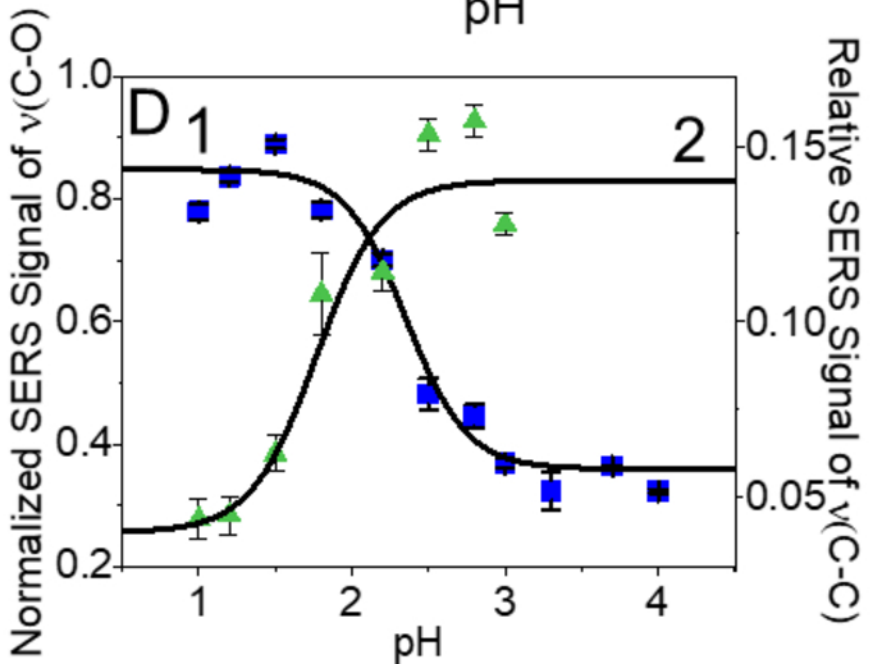
D
1
2
Normalized SERS Signal of ν(C-O)
Relative SERS Signal of ν(C-C)
1.0
0.8
0.6
0.4
0.2
0.15
0.10
0.05
1
2
3
4
pH

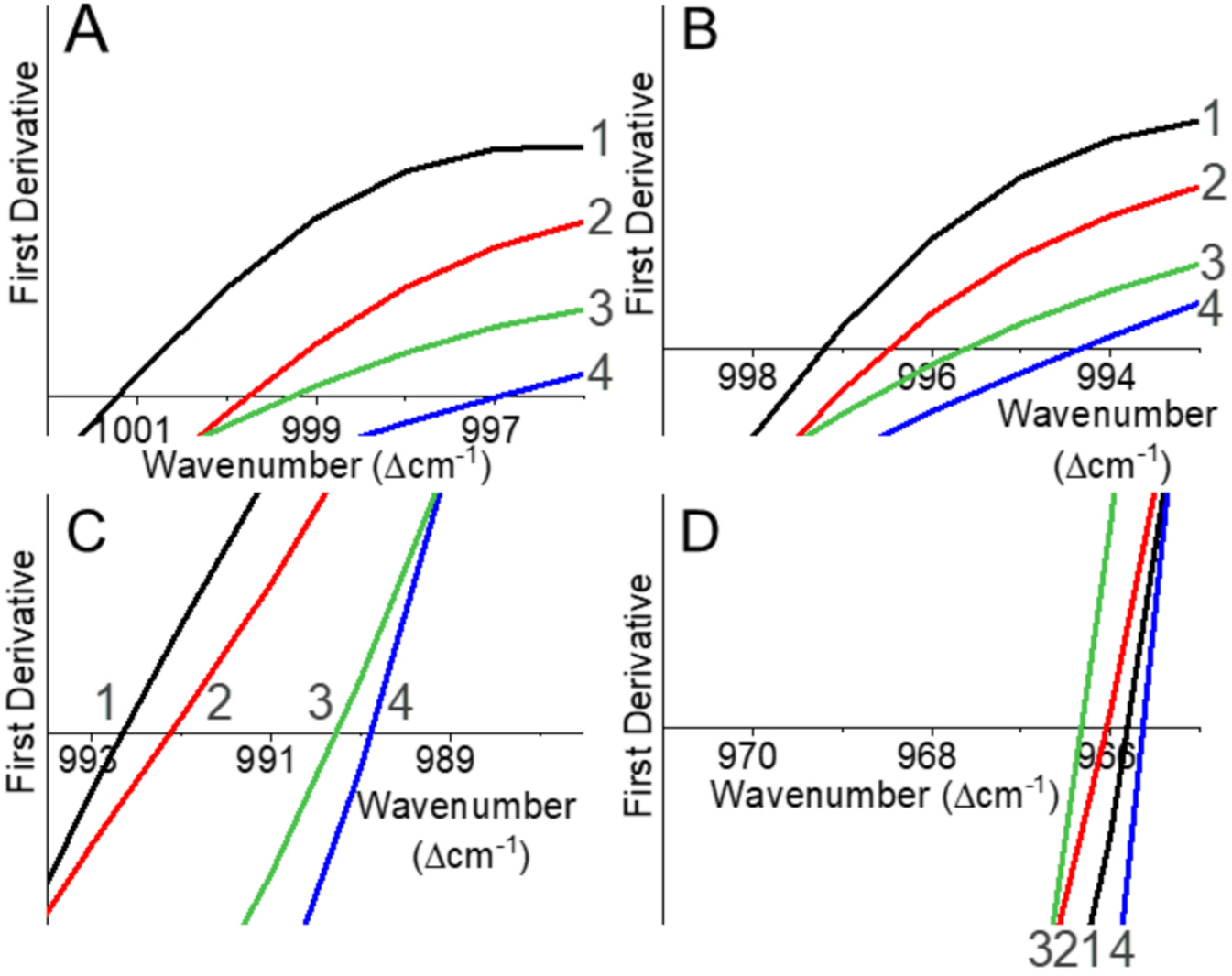
A
First Derivative
1
2
3
4
1001
999
997
Wavenumber (Δcm-1)
B
First Derivative
1
2
3
4
998
996
994
Wavenumber
(Δcm-1)
C
First Derivative
1
2
3
4
993
991
989
Wavenumber
(Δcm-1)
D
First Derivative
970
968
966
Wavenumber (Δcm-1)
3214

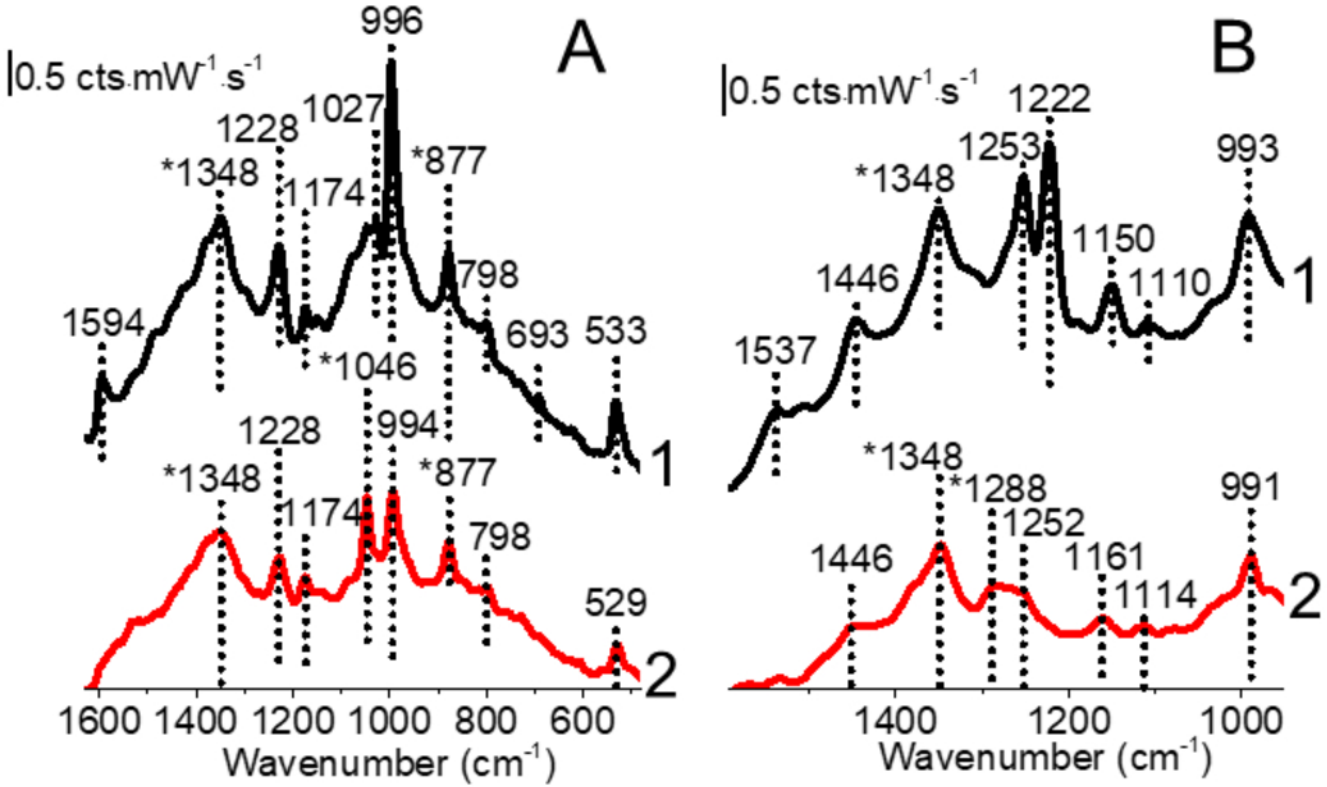
A
0.5 cts·mW-1·s-1
996
1027
1228
*1348
1174
*877
798
1594
693
533
*1046
1
1228
994
*1348
1174
*877
798
529
2
1600 1400 1200 1000 800 600
Wavenumber (cm-1)
B
0.5 cts·mW-1·s-1
1222
1253
993
*1348
1150
1446
1110
1537
1
*1348
*1288
991
1252
1446
1161
1114
2
1400 1200 1000
Wavenumber (cm-1)

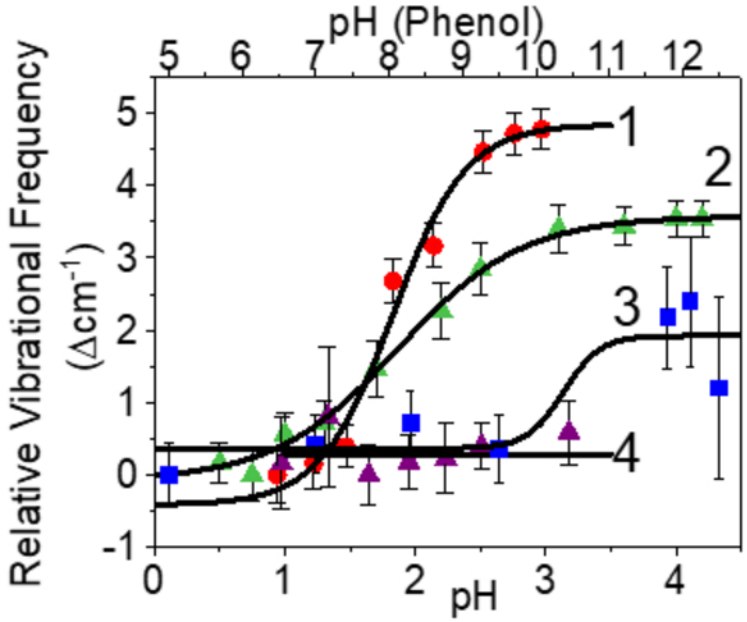
pH (Phenol)
5
6
7
8
9
10
11
12
Relative Vibrational Frequency
(Δcm-1)
5
4
3
2
1
0
-1
0
1
2
3
4
pH
1
2
3
4

Structure and Proposed Orientation	$pH < pK_{a,\ surf}$ Binding affinity (kcal/mol)	$pH > pK_{a,\ surf}$ Binding affinity (kcal/mol)
Benzoic Acid/Benzoate	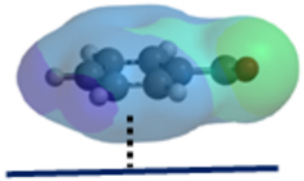 < 2.72 (±0.38)	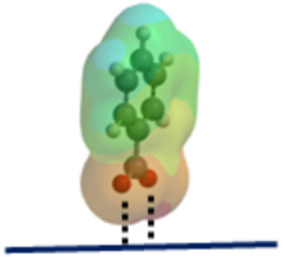 2.72 (±0.38)
Anilinium/ Aniline	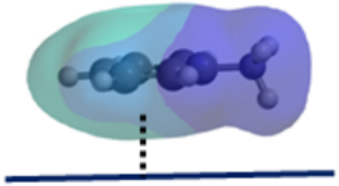 > 3.69 (±0.06)	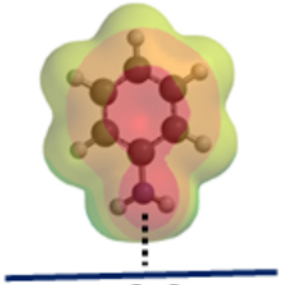 6-8
Phenol/ Phenoxide	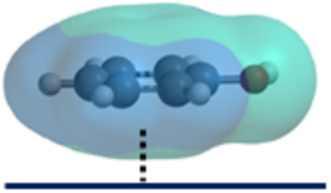 < 3.69 (±0.06)	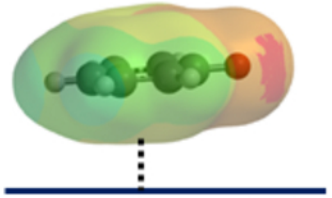 < 3.69 (±0.06)